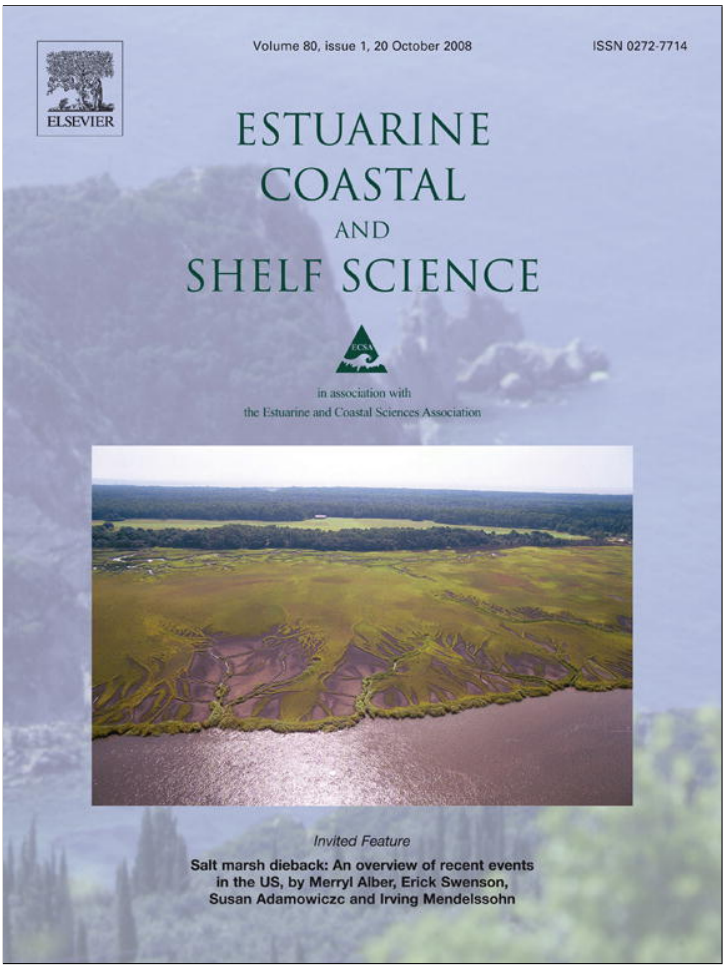

Estuarine, Coastal and Shelf Science 80 (2008) 141–152

Contents lists available at ScienceDirect

Estuarine, Coastal and Shelf Science

journal homepage: www.elsevier.com/locate/ecss

Stormwater plume detection by MODIS imagery in the southern California coastal ocean

Nikolay P. Nezlin [a,*], Paul M. DiGiacomo [b], Dario W. Diehl [a], Burton H. Jones [c], Scott C. Johnson [d], Michael J. Mengel [e], Kristen M. Reifel [c], Jonathan A. Warrick [f], Menghua Wang [b]

[a] Southern California Coastal Water Research Project (SCCWRP), Costa Mesa, CA 92626, USA
[b] NOAA/NESDIS Center for Satellite Applications and Research (STAR), Camp Springs, MD 20746, USA
[c] Department of Biological Sciences, University of Southern California, Los Angeles, CA 90089, USA
[d] Aquatic Bioassay and Consulting Laboratories, Ventura, CA 93001, USA
[e] Orange County Sanitation District (OCSD), Fountain Valley, CA 92728, USA
[f] USGS Coastal and Marine Geology Program, Santa Cruz, CA 95060, USA

ARTICLE INFO

Article history:
Received 2 February 2008
Accepted 15 July 2008
Available online 23 July 2008

Keywords:
ocean color
sea-spectral reflectance
MODIS
plumes
southern California Bight
32°00'–34°30'N, 120°00'–117°00'W

ABSTRACT

Stormwater plumes in the southern California coastal ocean were detected by MODIS-Aqua satellite imagery and compared to ship-based data on surface salinity and fecal indicator bacterial (FIB) counts collected during the Bight'03 Regional Water Quality Program surveys in February–March of 2004 and 2005. MODIS imagery was processed using a combined near-infrared/shortwave-infrared (NIR-SWIR) atmospheric correction method, which substantially improved normalized water-leaving radiation (nLw) optical spectra in coastal waters with high turbidity. Plumes were detected using a minimum-distance supervised classification method based on nLw spectra averaged within the training areas, defined as circular zones of 1.5–5.0-km radii around field stations with a surface salinity of $S < 32.0$ ("plume") and $S > 33.0$ ("ocean"). The plume optical signatures (i.e., the nLw differences between "plume" and "ocean") were most evident during the first 2 days after the rainstorms. To assess the accuracy of plume detection, stations were classified into "plume" and "ocean" using two criteria: (1) "plume" included the stations with salinity below a certain threshold estimated from the maximum accuracy of plume detection; and (2) FIB counts in "plume" exceeded the California State Water Board standards. The salinity threshold between "plume" and "ocean" was estimated as 32.2. The total accuracy of plume detection in terms of surface salinity was not high (68% on average), seemingly because of imperfect correlation between plume salinity and ocean color. The accuracy of plume detection in terms of FIB exceedances was even lower (64% on average), resulting from low correlation between ocean color and bacterial contamination. Nevertheless, satellite imagery was shown to be a useful tool for the estimation of the extent of potentially polluted plumes, which was hardly achievable by direct sampling methods (in particular, because the grids of ship-based stations covered only small parts of the plumes detected via synoptic MODIS imagery). In most southern California coastal areas, the zones of bacterial contamination were much smaller than the areas of turbid plumes; an exception was the plume of the Tijuana River, where the zone of bacterial contamination was comparable with the zone of plume detected by ocean color.

1. Introduction

This study is focused on developing the ability to routinely detect and classify stormwater runoff plumes in the Southern California Bight (SCB) for the purposes of synoptic water quality assessments in this region. Plumes are identified as water masses with decreased salinity relative to ambient ocean water. Such gradients in salinity can only be presently measured through in situ measurements. Salinity cannot yet be measured from space (nor in the foreseeable future with necessary resolution for coastal applications), although a high correlation between salinity and "ocean color" parameters has been shown in many coastal regions (Monahan and Pybus, 1978; Vasilkov et al., 1999; Siddorn et al., 2001; Miller and McKee, 2004). The color of plumes results from high concentrations of suspended sediments and Colored Dissolved Organic Matter (CDOM). Suspended sediments increase backscattering in the longer wavelength portion of the visible spectrum (Toole and Siegel, 2001; Miller et al., 2005); CDOM absorbs light at

* Corresponding author.
E-mail address: nikolayn@sccwrp.org (N.P. Nezlin).

0272-7714/$ – see front matter © 2008 Elsevier Ltd. All rights reserved.
doi:10.1016/j.ecss.2008.07.012

short wavelengths (Del Castillo, 2005) and CDOM concentration is more conservative than suspended sediments. Emerging plumes contain high concentrations of suspended sediments, which rapidly decrease with time due to gravitational sedimentation (Warrick et al., 2004b; Ahn et al., 2005). Decreases in CDOM occur due to photodegradation, but this process takes weeks to months (Vodacek et al., 1997; Opsahl and Benner, 1998).

Ocean color satellite imagery could be used to estimate when and where high concentrations of contaminants occur, because concentrations of contaminants in stormwater plumes (e.g., fecal indicator bacteria) are related to salinity (Bay et al., 2003; Nezlin et al., 2007 Chapter 6), which, in turn, can be related to ocean color. This information would be especially useful to coastal managers and governing agencies who are required to perform additional monitoring and close beaches if contaminants exceed various standards (State Water Resources Control Board, 2005).

Previous studies of stormwater plumes based on ocean color satellite imagery were focused on physical forcing regulating plume dynamics (e.g., Estournel et al., 1997; Froidefond et al., 1998; Siegel et al., 1999; Warrick and Fong, 2004; Warrick et al., 2007) and/or estimation of the amount of discharged sediments (e.g., Lira et al., 1997; Ouillon et al., 1997; Warrick et al., 2004a,b). In southern California, previous studies (e.g., the "Plumes and Blooms" program) studied spatial and temporal characteristics of the plumes of discharged sediment and associated with them phytoplankton blooms in the Santa Barbara Channel (Toole and Siegel, 2001; Otero and Siegel, 2004). Our previous satellite-based plume studies (e.g., Nezlin and DiGiacomo, 2005; Nezlin et al., 2005) focused primarily on multi-year analysis of plume dynamics, whereas the present effort is geared toward developing an event detection, classification and impact assessment system for near-real time satellite-based synoptic characterizations of water quality. The results of this study could be used to develop a cost-effective water quality monitoring strategy in the SCB and other urban coastal regions that would provide environmental managers with information on coastal water quality that is both faster and spatially more extensive than the exclusively in situ, shipboard sampling techniques currently in use. However, such satellite-based information would merely complement, and not eliminate, field based sampling efforts.

Analyzing the accuracy of plume detection, we separately assess the accuracy statistics for "plume" (i.e., potentially polluted waters) and "ocean" (i.e., potentially clean waters). For both "plume" and "ocean", we have commission and omission errors (see Congalton and Green, 1999; Lillesand and Kiefer, 2000). Commission error is the chance to erroneously include wrong pixels into a class. Omission error is the chance to lose pixels by including them into other classes. Commission error for "plume" and omission error for "ocean" indicate the chance to erroneously detect a plume (and, potentially by extension, recommend a beach closure) in the absence of contamination; the consequences of this kind of inaccuracy can be economic losses for recreation industry. In contrast, omission error for "plume" and commission error for "ocean" indicate the chance to miss contaminated plume waters, resulting in potential health risks for beach visitors.

For this study, we processed satellite images collected by the Moderate Resolution Imaging Spectroradiometer (MODIS) on the Aqua satellite platform during the Bight'03 Regional Water Quality Program surveys in February–March of 2004 and 2005 using the combined near-infrared/shortwave-infrared (NIR-SWIR) method of atmospheric correction (Wang and Shi, 2007), which was developed especially for analysis of coastal data. We compared optical signatures (i.e., the spectra of normalized water-leaving radiances, nLw) in the plume core (surface salinity $S < 32.0$), plume edge ($32.0 \leq S \leq 33.0$) and ocean ($S > 33.0$) waters. Then, we used the averaged optical signatures of the plume core and ocean as endmembers (training areas) to classify all pixels from the MODIS-Aqua imagery into two classes: "plume" and "ocean". To estimate the accuracy of classification we used the entire range of S measurements, including plume core, plume edge, and ocean. Also, we used California State Water Board fecal indicator bacteria (FIB) exceedance standards as another measure of plume detection accuracy. Finally, we assessed plume area size and compared the plumes detected from remotely sensed ocean color with the plumes detected in terms of decreased salinity and bacterial contamination.

2. Stormwater plumes in the Southern California Bight

Stormwater plumes are a main source of pollution in the southern California (SC) coastal ocean. Noble et al. (2003) found that 96% of the shoreline met water quality standards during dry weather, but 58% of the shoreline failed to water quality standards during wet weather. The rainy season in SC occurs from late fall to early spring (Dailey et al., 1993) and consists of episodic storm events, which contribute more than 95% of the total annual runoff to the SCB (Schiff et al., 2000). SC is a highly developed urban area, where increased impervious surface area leads to greater runoff and contaminant loading to the ocean, producing up to 90% more runoff than unaltered watersheds (Miller et al., 2002). Rapid surface flow following rainstorms results in plumes emerging and increasing to a maximum size during a short (1–2 days) period after these storms (Nezlin et al., 2005).

The optical signatures of plumes in SC result to a large extent from high concentrations of suspended sediments and CDOM discharged with stormwater (Mertes and Warrick, 2001; Warrick and Milliman, 2003; Warrick et al., 2004c). Resuspension of sediments from the ocean bottom does not play a significant role in the SCB, because the continental shelf is narrow. Washburn et al. (1992) studied resuspension in the western part of the San Pedro Shelf and only observed high concentrations of sediments resuspended by water circulation within 15 m of the bottom. Throughout the SCB, the ocean bottom exceeds 15 m within 1 km offshore; as such, the sediments resuspended from the bottom by winds, waves, and currents are not likely to be a significant factor for purposes of this analysis.

The propagation, direction, and persistence of stormwater plumes in the SCB are variable, depending on locally and remotely modulated circulation patterns (Nezlin and DiGiacomo, 2005). Alongshore movement of stormwater plumes in the SCB prevails over across-shore movement (Warrick et al., 2007). Downcoast propagation of plumes is typical of the spring period and results from wind-driven upwelling-favorable coastal circulation associated with a spring transition (Strub et al., 1987; Strub and James, 1988; Lynn et al., 2003).

3. Methods

Ship-based data and MODIS imagery were collected during the Bight'03 Regional Water Quality Program surveys in February–March of 2004 and 2005 (see Warrick et al., 2007). Due to the inconsistent nature of rainfall within SC, sampling was carried out in two sub-regions, north/central and south (San Diego), independent of each other. Sampling event #1 was initiated by the storms February 22–23, 2004 in the San Diego area and 3 days later, on February 25–26, in the northern and central areas. Sampling event #2 was initiated on February 11–12, 2005 in the San Diego area and almost 6 weeks later, on March 23, 2005 in the northern and central areas. In this study, we analyzed the observations collected during 8 days when both the satellite images and ship-based sampling were available: February 24, 27–29, and March 1, 2004 and February 13, March 23 and 25, 2005.

The satellite data used in this study were collected by the NASA MODIS sensor operating onboard the near-polar sun-synchronous satellite platform Aqua orbiting at 705-km altitude (Esaias et al., 1998). Aqua passes the equator south to north at ~13:30 local time; as such, all the images were acquired within 2 h after local noon (20:00–22:00 UTC). The MODIS sensor collects data in 36 spectral bands, from 400 to 14,000 nm; of which only some are useful for ocean applications. The radiances measured by the satellite sensors were converted into normalized water-leaving radiances (nLw). The nLw parameter is defined to be the upwelling radiance just above the sea surface, in the absence of an atmosphere, and with the sun directly overhead (Gordon and Wang, 1994).

In this study, MODIS imagery was processed using a combined NIR-SWIR atmospheric correction approach (Wang and Shi, 2007). The traditional method of atmospheric correction used for processing of Sea-viewing Wide-Field-of-view Sensor (SeaWiFS) and MODIS imagery is based on two NIR bands used for identifying aerosol type and correcting aerosol contributions at the visible wavelengths (Gordon and Wang, 1994; Gordon, 1997). For MODIS, two NIR bands centered at 748 and 869 nm are used and the ocean is assumed to be black at these two wavelengths. This assumption works well for open ocean waters. In turbid coastal waters, however, ocean contribution to NIR is significant, resulting in substantial errors in derived ocean color products (Wang and Shi, 2005). In this case, two SWIR bands (e.g., 1240 and 2130 nm) are preferable for atmospheric correction, because ocean surface reflectance in SWIR is close to zero regardless of suspended matter and CDOM concentrations (Wang, 2007; Wang et al., 2007). However, the MODIS SWIR were designed for the land and atmosphere applications with substantially lower sensor band signal-noise ratio (SNR) values. For accurate ocean color products, much better sensor SNR values for the SWIR bands are required (Wang, 2007). Thus, we used a combined NIR-SWIR method (Shi and Wang, 2007; Wang and Shi, 2007) for the MODIS ocean color data processing.

In the combined NIR-SWIR method of atmospheric correction, a turbidity index (Shi and Wang, 2007) based on MODIS-measured radiances at the NIR and SWIR bands is computed to discriminate between turbid coastal and non-turbid ocean waters. For the pixels identified as turbid waters, the SWIR method of atmospheric correction is applied; for non-turbid waters, the NIR method is used (see details in Wang and Shi, 2007). Previous studies illustrated that this approach results in good quality ocean color products without obvious discontinuities (Wang and Shi, 2007).

The nLw radiances were estimated at the eight MODIS ocean visible and NIR wavelengths: 412, 443, 488, 531, 551, 667, 678, and 748 nm. MODIS pixel size is ~1 km. The pixels associated with atmospheric correction failure, land, cloud or ice, stray light, and sun glint were excluded from analysis. We also masked the pixels with L2 flags for "shallow water", "aerosol iterations exceeded maximum", "atmospheric correction is suspect", and "high degree of polarization".

Ship-based samples were collected in four geographic regions that represent the river mouths of the largest southern California watersheds (Fig. 1). These regions included (from the north): the eastern Santa Barbara Channel (Santa Clara and Ventura Rivers); Santa Monica Bay (Ballona Creek); the San Pedro Shelf (Los Angeles, San Gabriel and Santa Ana Rivers and Newport Bay); and the southern Bight (San Diego and Tijuana Rivers). Sampling occurred on regularly spaced grids for each region. The primary intent of the grids was to sample the nearshore discharge areas and assess water quality there, not necessarily to track plumes as they advected away from the river mouth regions. The primary method of investigation was shipboard profiling of the plumes with an enhanced CTD system (conductivity, temperature, depth, dissolved oxygen, pH, transmissometer, chlorophyll fluorometer, and CDOM fluorometer),

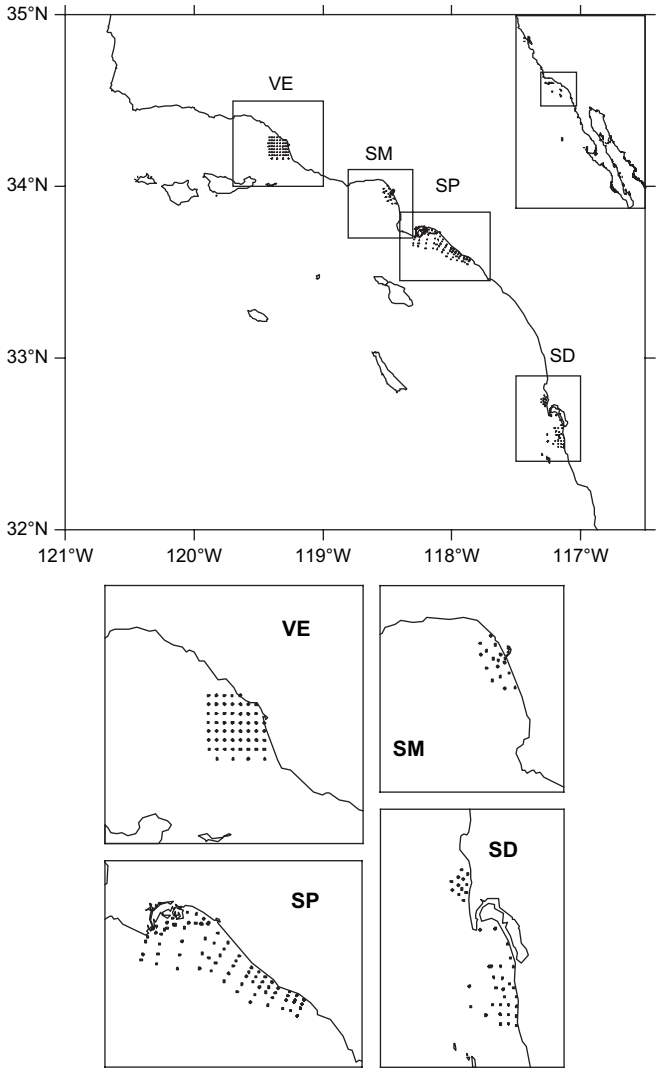

Fig. 1. Stations for ship-based sampling during the Bight'03 Program in four regions in the Southern California Bight: Ventura (VE); Santa Monica Bay (SM); San Pedro Shelf (SP); San Diego (SD).

hereafter referred to as CTD+. Water samples were taken at 1-m water depth for most sites and at subsurface depths below the buoyant plume for a limited number of sites. Samples were analyzed for total suspended solids, chlorophyll, macronutrients (Si, N, P), FIB (total coliforms, fecal coliforms, and *Enterococcus*) and toxicity. Here we focus on surface salinity (derived from CTD+ conductivity) and FIB. The stations were classified as exceeding California State Water Board standards when the FIB counts in single sample were >10,000 for total coliforms; >400 for fecal coliforms; and >104 for *Enterococcus* (State Water Resources Control Board, 2005).

All ship-based stations were classified into plume core ($S < 32.0$), plume edge ($32.0 \le S \le 33.0$) and ocean ($S > 33.0$) assuming normal ocean salinity in the SCB as 33.4–33.6 (Hickey, 1993). Optical spectra (nLw) were selected from MODIS images collected during the same day as ship-based sampling from circles of 1.5-km radius centered on the location of each ship-based station. Masked pixels from MODIS imagery were excluded from statistical computations. For each nLw (412–748 nm), median and quartile (25% and 75%) statistics were calculated for each class. Optical spectra (nLw medians) of plume cores ($S < 32.0$) and ocean ($S > 33.0$) were used as endmembers (training areas) for supervised classification.

A minimum distance supervised classification technique (Richards, 1999) used the mean vectors of each endmember (i.e., eight nLw vectors of plume and ocean water, respectively) and calculated the Euclidean distance from each image pixel to the mean vector for each class. Each pixel from the MODIS image was classified to the nearest class (i.e., "plume" or "ocean"). The accuracy of classification was assessed comparing the MODIS imagery pixels selected from the circles of variable size (radii $R = 1.5$–5.0 km) centered on the location of each ship-based station with the classes ("plume" or "ocean") to which these stations were attributed based on surface salinity or FIB exceedances. Various R was used for two reasons: first, satellite navigation may not be accurate to a pixel (see Bailey and Werdell, 2006) and the level of this kind of spatial inaccuracy is uncertain. Second, we have to take into account the time lag between ship-based data collection (surveys typically were from 7 a.m. to 4 p.m. local time) and MODIS-Aqua imagery (taken about 1–2 p.m.). A horizontal velocity of 50 cm s^{-1} (equal to $\sim$1.8 km h^{-1}) such as observed in southern California river plumes (Warrick et al., 2007) can move the plume boundary as far as 5–10 km during a few hours, which can dramatically increase spatial inaccuracy between water surface parcels measured by satellites and from research vessels. We used different R values when selecting the pixels from the classified MODIS imagery to check which R value corresponds to maximum classification accuracy (see Results).

To assess the accuracy of classification in terms of salinity, we used a larger set of salinity data than the data set used for endmember estimation. In addition to "plume core" and "ocean", this data set included the stations attributed to "plume edge" ($32.0 \leq S \leq 33.0$). We used different S thresholds between "plume" and "ocean" and selected the S value resulting in maximum total accuracy.

As accuracy measures, we used total accuracy, commission and omission errors for "plume" and "ocean" classes, and KHAT statistic (Congalton and Green, 1999; Lillesand and Kiefer, 2000). Total accuracy is the percentage of correctly classified pixels. KHAT is a statistical measure of the difference between the actual total classification accuracy and the erroneous accuracy measure that could be obtained by completely random assignments of pixels to classes. The commission error for "plume" and the omission error for "ocean" both illustrate the number of pixels erroneously included into "plume" instead of "ocean" (N-lost); however, these statistics are not equal, because the "plume" commission error is N-lost divided by the total number of pixels in "plume" class and the "ocean" omission error is N-lost divided by the total number of pixels in the "ocean" class.

4. Results

4.1. Optical spectra of stormwater plumes

The optical signatures of the plume core, plume edge, and ocean were significantly different (Fig. 2; Table 1) and these differences could be explained by backscattering of suspended sediments and absorption of CDOM. At longer wavelengths (488–748 nm), nLw in the plume core exceeded nLw in ocean waters; this difference looked like a result of backscattering of suspended sediments. At 412 nm, nLw in plumes was lower when compared with ocean waters, which could potentially be explained by CDOM absorption. In plume edge waters, the shape of nLw spectrum was similar to the plume core, but nLw was lower at all wavelengths, excluding the shortest 412 nm (Fig. 2; Table 1), suggesting that in the plume edge the optical components affecting remotely sensed reflectance are the same than in the plume core but just diminished in concentration.

The optical signatures of the plumes changed with time (Fig. 2; Table 1). During the first 2 days after storm events, the difference between the plume core and the ocean was similar to the pattern revealed on the basis of all observations. The optical spectrum of the plume edge, however, during days 1–2 after the storm was much closer to the plume core than during the next 2 days. We explain this with the presence of high sediment and CDOM concentrations in the plume (including both core and edge) during a short period after the plume emergence. During the next 3–4 days, the optical spectrum of the ocean remained unchanged, but the spectra of the plume core and the plume edge changed. In the plume, all nLw decreased consistent with decrease of the suspended sediments concentration and mixing. CDOM concentration in the plume remained high, and the relative contribution of the CDOM signal into the plume optical signature at short wavelengths (412 and 443 nm) increased. At the plume edge, nLw at wavelengths >488 nm was lower than in the plume core as would be expected with lower concentration of suspended sediments.

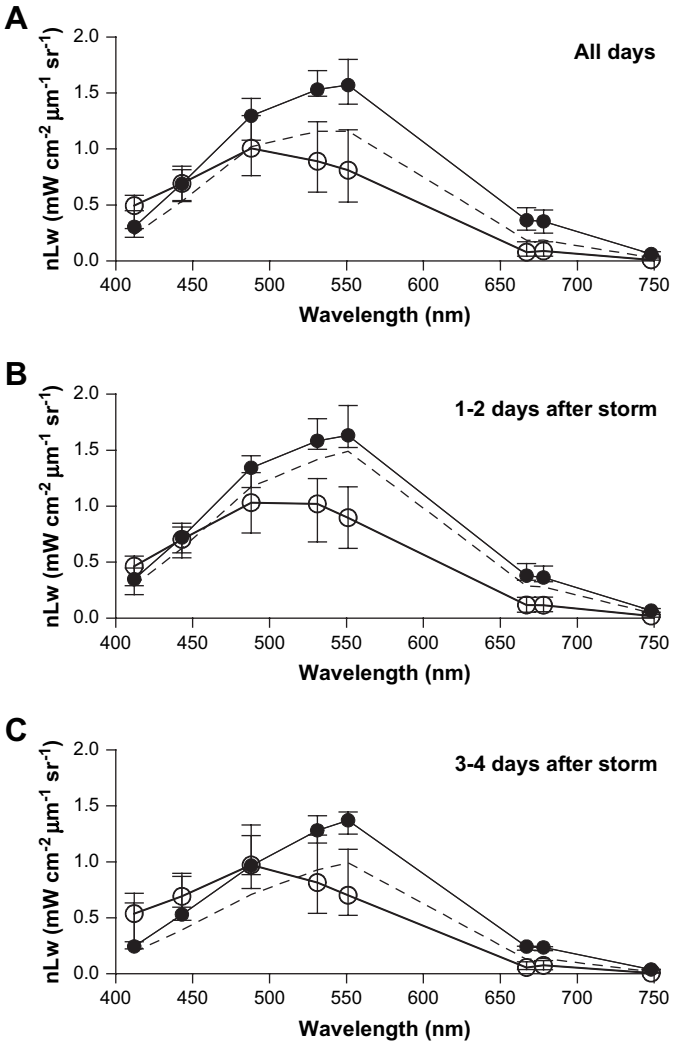

Fig. 2. Normalized water-leaving radiation (nLw) spectra of the plume core ($S < 32.0$; black circles), plume edge ($32.0 \leq S \leq 33.0$; dashed line), and ocean waters ($S > 33.0$; open circles) averaged over all observations (A), first-second (B) and third-fourth (C) days after rainstorm.

4.2. Accuracy of plume detection

The best accuracy of classification was achieved when the S threshold between "plume" and "ocean" was 32.2. We tested different S thresholds within the range 32.0–33.0 and various R (the

Table 1
The sign and significance of differences (p) based on Mann–Whitney U-test between nLw in plume core (PC; $S < 32.0$), plume edge (PE; $32.0 \leq S \leq 33.0$) and ocean (OC; $S > 33.0$) in all observations, 1–2 days and 3–4 days after rainstorm (the actual values are presented in Fig. 2). Number of stations in PC, PE and OC: total – 22, 89 and 64; 1–2 days after rainstorm – 18, 55 and 31; 3–4 days after rainstorms – 4, 34 and 33, respectively. (+/−) means that nLw in the first class (PC, PE or OC) was significantly higher/lower than nLw in the second class; (=) means that the differences were insignificant ($p > 0.05$)

nLw (nm)	All days			1–2 days after rainstorm			3–4 days after rainstorm		
	PC > OC	PC > PE	PE > OC	PC > OC	PC > PE	PE > OC	PC > OC	PC > PE	PE > OC
412	(−) 0.007	(=) 0.218	(−) 0.000	(=) 0.078	(=) 0.578	(−) 0.000	(=) 0.195	(=) 0.134	(−) 0.000
443	(=) 0.984	(+) 0.024	(−) 0.004	(=) 0.561	(=) 0.101	(=) 0.276	(=) 0.525	(=) 0.083	(−) 0.005
488	(+) 0.004	(+) 0.003	(=) 0.959	(+) 0.004	(+) 0.023	(=) 0.161	(=) 0.769	(=) 0.083	(=) 0.087
531	(+) 0.000	(+) 0.001	(+) 0.000	(+) 0.000	(+) 0.020	(+) 0.001	(=) 0.078	(=) 0.064	(=) 0.142
551	(+) 0.000	(+) 0.001	(+) 0.000	(+) 0.000	(+) 0.023	(+) 0.000	(+) 0.031	(+) 0.036	(+) 0.010
667	(+) 0.000	(+) 0.000	(+) 0.000	(+) 0.000	(+) 0.007	(+) 0.000	(+) 0.013	(+) 0.024	(+) 0.000
678	(+) 0.000	(+) 0.000	(+) 0.000	(+) 0.000	(+) 0.007	(+) 0.000	(+) 0.015	(+) 0.025	(+) 0.000
748	(+) 0.000	(+) 0.000	(+) 0.000	(+) 0.000	(+) 0.009	(+) 0.000	(+) 0.011	(+) 0.017	(+) 0.000

radii of circular areas centered at ship-based station coordinates within which image pixels were selected for accuracy assessments) within the range 1.5–5.0 km. At $S = 32.2$ the total accuracy of classification reached its maximum (67–70%) and was almost independent of R. Other statistics, however, indicated that best accuracy was at $R = 1.5$ km. KHAT (i.e., the statistical significance of total accuracy at the given number of classes and measurements) decreased from 31% at $R = 1.5$ km to 24% at $R = 5.0$ km (Fig. 3a). Plume omission error was larger than other statistics dependent on R, increasing from 14% at $R = 1.5$ km to 33% at $R = 5.0$ km. The latter statistic is especially important in water quality analysis, because it illustrates the chance to miss a polluted plume that could result in human health risk.

The accuracy of plume detection in terms of FIB exceedances was lower than in terms of salinity (Fig. 3b). The total accuracy was 64–68%; KHAT decreased from 21% at $R = 1.5$ km to 18% at $R = 5.0$ km. Plume omission error was low (13%) at $R = 1.5$ km and increased to 37% at $R = 5.0$ km. As such, we conclude that minimum R (i.e., 1.5 km) is the best for accuracy analysis.

Combining both salinity and FIB data in plume detection somewhat improved the accuracy statistics. When plumes were designated as the stations where either salinity was less than 32.2 or FIB counts exceeded standards, both total accuracy and KHAT slightly increased (71% and 38%, respectively).

4.3. Stormwater plumes in SCB

The results of the classification showed robust plume patterns located along the coast and associated with river mouths (Figs. 4–6). The plume areas obtained from the satellite imagery significantly exceeded the areas covered by the ship-based surveys, whose station grids were not intended to capture the entire regional plumes given the time, expense, and difficulty that would result from such an effort. In the Ventura region, the sampled area was restricted to the zone near the mouths of the Santa Clara and Ventura rivers, while the signature of the turbid plume extended downcoast, especially in March 2005 (Fig. 4). Plume signatures from local discharges into Santa Monica Bay were small, but in March 2005, the tip of a large plume from the Ventura and Santa Clara rivers was transported to the western part of Santa Monica Bay. On the San Pedro Shelf in February 2004, the plume also propagated downcoast beyond the area of the ship-based surveys (Fig. 5). In spring 2005, the plume signature was not observed after the rainstorm (March 23) due to cloud cover; 2 days later (March 25) the plume was very small. A small plume was observed in the mouth of the San Diego River in February 28–29, 2004 and February 13, 2005 (Fig. 6). The plume of the Tijuana River was much larger; in the image on February 24, 2004, it propagated upcoast; in other images its direction was southward.

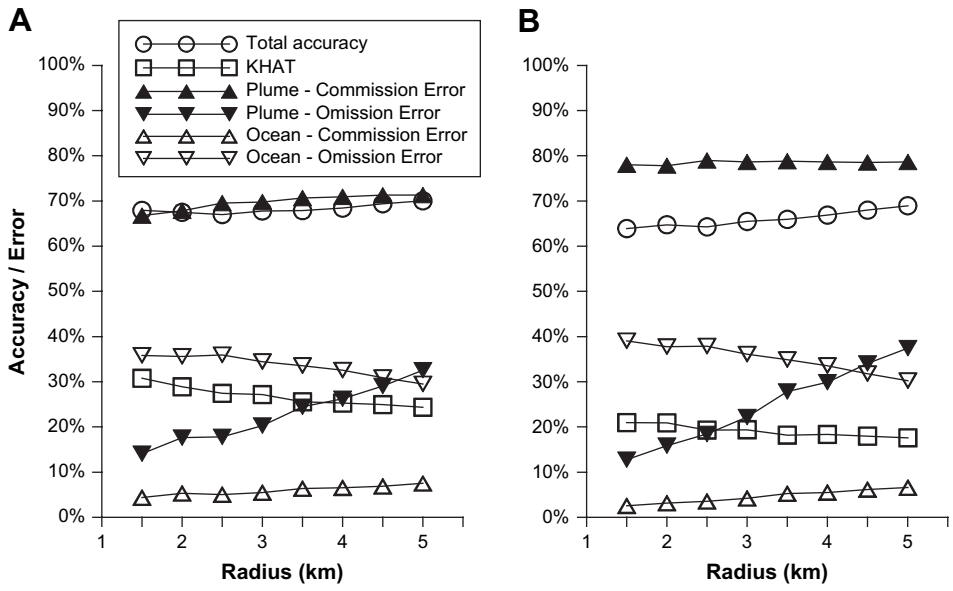

Fig. 3. Accuracy statistics (total, KHAT, commission and omission errors of "plume" and "ocean") of plume detection based on (A) salinity (the threshold between "plume" and ocean $S = 32.2$) and (B) FIB counts (the threshold between "plume" and "ocean" is California State Water Board Standards exceedance) depending on the radius (R) of the circle around each station where the classified pixels were selected.

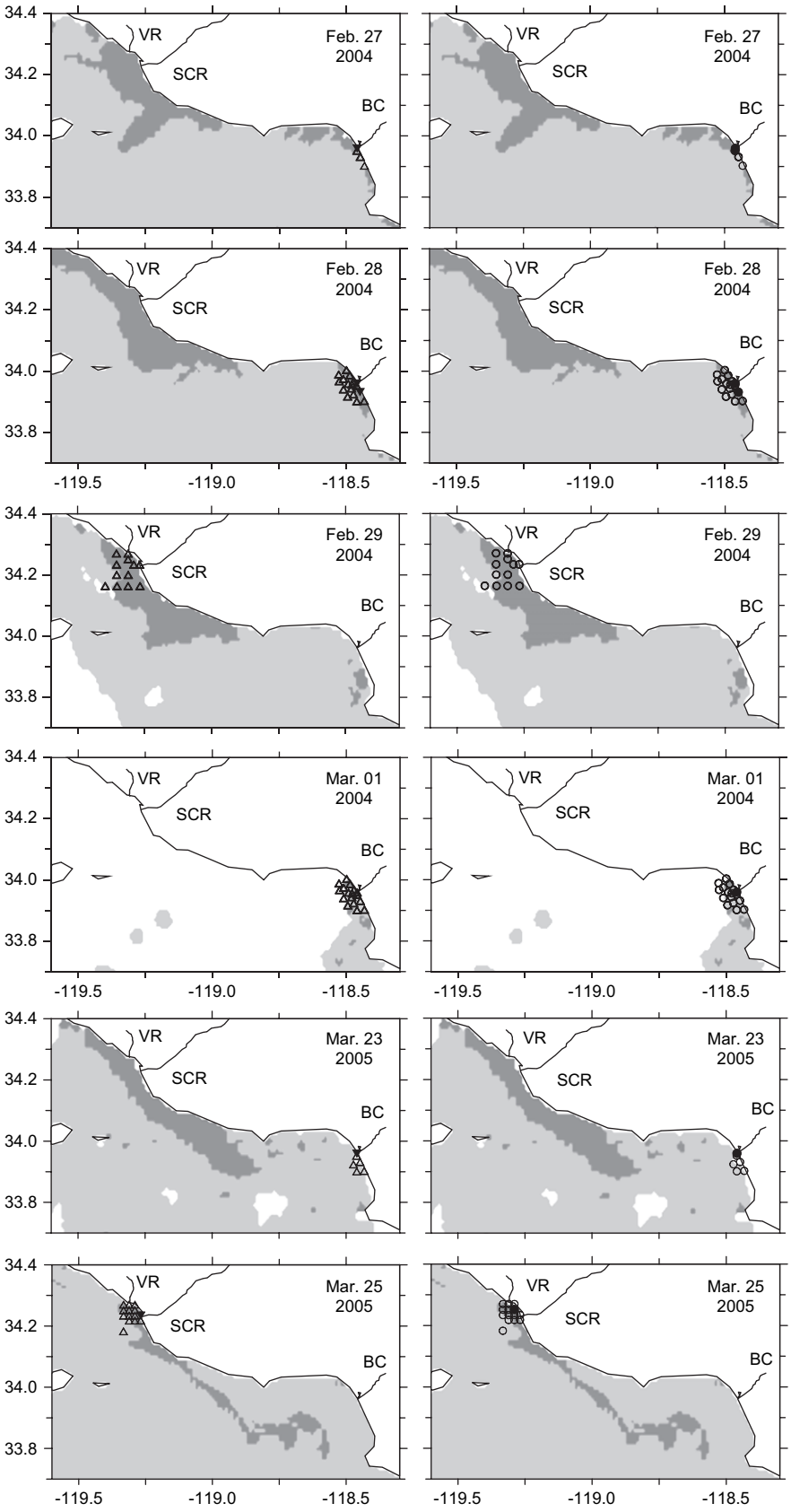

Fig. 4. Plume areas (dark shaded) in the Ventura and Santa Monica Bay regions resulting from classification of the MODIS imagery and the Bight'03 ship-based measurements of salinity and FIB counts. Light shading indicates ocean waters; white indicates the absence of MODIS imagery due to cloud cover. Black/white triangles (left) indicate bacterial counts exceeding/not exceeding California standards; black/white circles (right) indicate salinity exceeding/not exceeding 32.2. VR–Ventura River; SCR–Santa Clara River; BC–Ballona Creek.

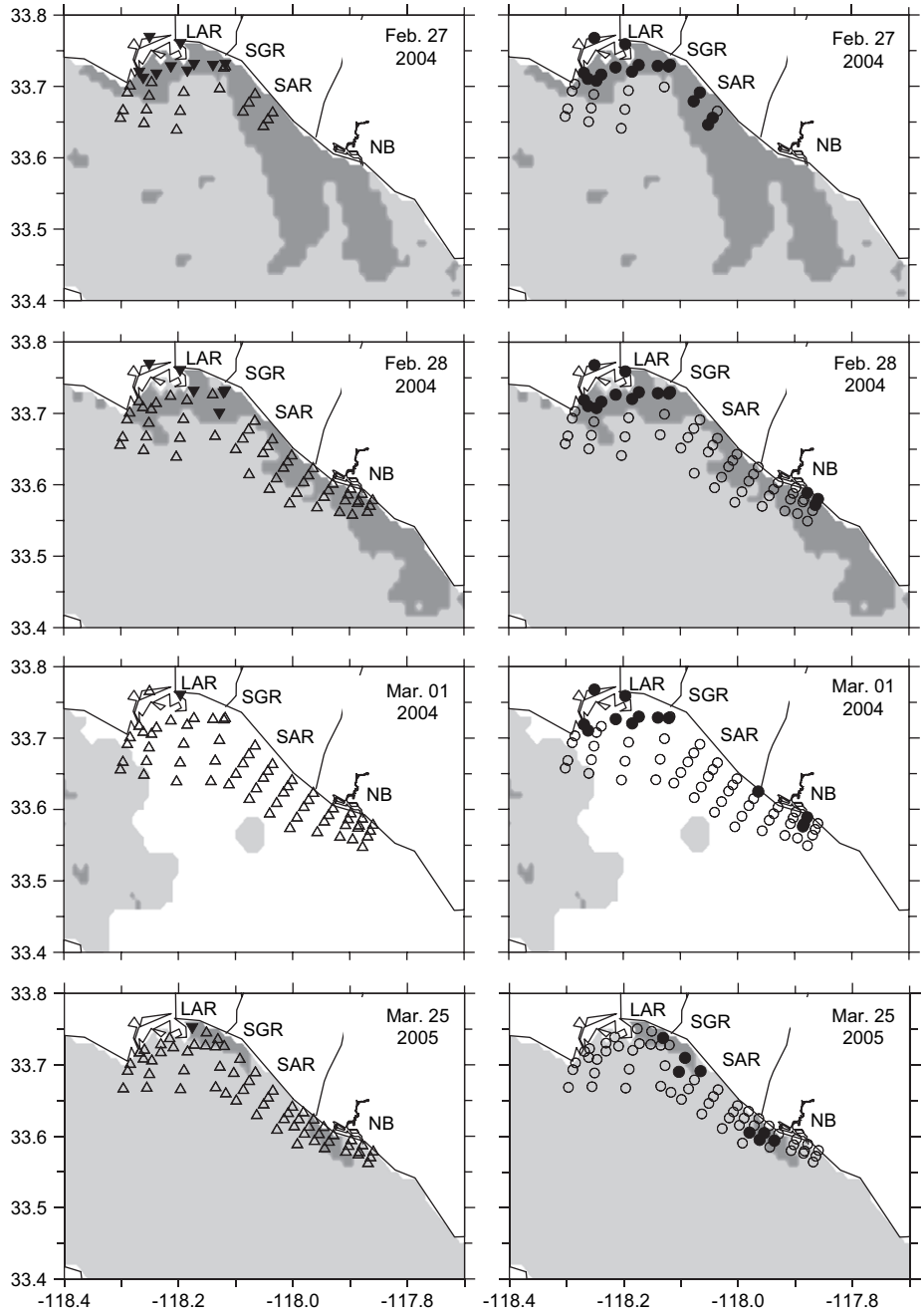

Fig. 5. Plumes on the San Pedro Shelf resulting from classification of the MODIS imagery and the Bight'03 ship-based measurements of salinity and FIB counts. For shadings and symbols see Fig. 4. LAR–Los Angeles River; SGR–San Gabriel River; SAR–Santa Ana River; NB–Newport Bay.

Plumes frequently extended upward of 10 km offshore (e.g., Fig. 4). Overall, the largest plume area size (692 km^2) was observed in the Ventura region on February 28, 2004 (Table 2). During other days when the sky was clear and a significant part of the Ventura region was observed by satellite, the plumes there were also large (409–669 km^2). Plumes of comparable size were observed on the San Pedro Shelf in February 2004 1–2 days after the storm (335–503 km^2); on the next day, however, the plume size substantially decreased (115 km^2).

Maximum size of the plumes in the Ventura and San Diego regions was observed on February 28, 2004, 2 days after a rainstorm (Table 2). In contrast, on the San Pedro Shelf, the maximum size of the combined plume of the Los Angeles, San Gabriel and Santa Ana rivers was observed 1 day earlier, on February 27, 2004. The higher speed of plume formation on the San Pedro Shelf resulted from more intensive runoff over impervious surfaces, because the watersheds adjacent to the San Pedro Shelf region are more developed (urbanized) as compared with more natural watersheds in the Ventura and San Diego regions (see Nezlin et al., 2005).

The plume areas estimated based on ocean surface color were significantly larger than the areas of impact calculated based on FIB exceedances by interpolating over the in situ sampling grid (Table 3). No impact in terms of bacterial contamination was estimated for the Ventura and Santa Monica Bay regions. For the San Pedro Shelf, the largest area of FIB impact was $<$40 km^2 (on the first day after the

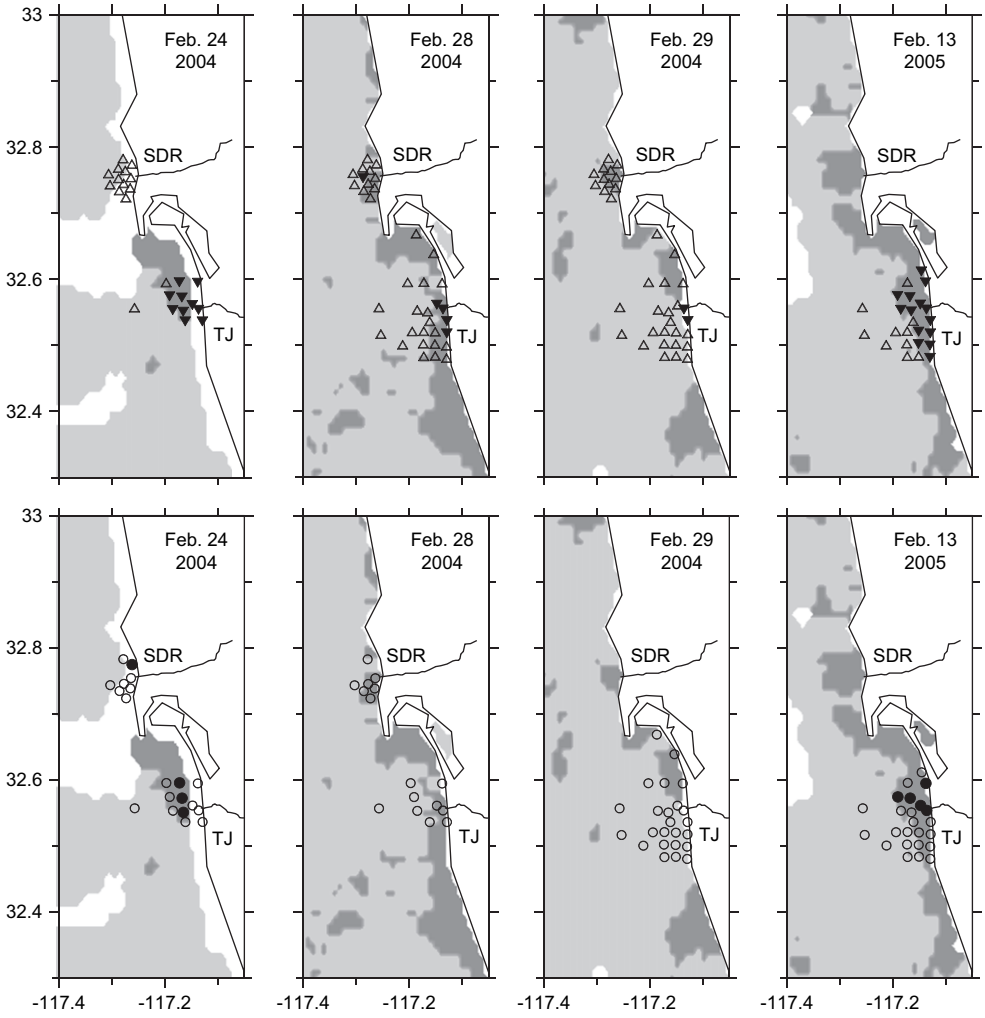

Fig. 6. Plumes in the San Diego region resulting from classification of the MODIS imagery and the Bight'03 ship-based measurements of salinity and FIB counts. For shadings and symbols see Fig. 4. SDR–San Diego River; TJ–Tijuana River.

storm), which was ~6% of the plume area estimated from ocean color. In the San Diego area, the impact of the Tijuana River was ~50 km^2 in 2004 and 50–100 km^2 in 2005 (cf. Fig. 6). The plume of the Tijuana River estimated from ocean color was 87–324 km^2 (Table 2); as such, the area of FIB impact was comparable with the plume observed by satellite.

Table 2
Plume areas (km^2) estimated from MODIS-Aqua imagery classified on the basis of Bight'03 ship-based sampling. Regions indicate outfalls of the rivers: SCR–Santa Clara River; VR–Ventura River; BC–Ballona Creek; LAR–Los Angeles River; SGR–San Gabriel River; SAR–Santa Ana River; NB–Newport Bay; SDR–San Diego River; TJR–Tijuana River

Date	Day after storm	Regions				
		Ventura (SCR + VR)	Santa Monica Bay (BC)	San Pedro (LAR + SGR + SAR + NB)	San Diego (SDR)	San Diego (TJR)
Feb. 24, 2004	1[a]	–	–	–	0	87
Feb. 27, 2004	1	578	117	503	0	130
Feb. 28, 2004	2	692	53	335	19	324
Feb. 29, 2004	3	603	51	115	15	124
Mar. 01, 2004	4	–	34	–	–	–
Feb. 13, 2005	1[a]	–	–	–	54	240
Mar. 23, 2005	1	669	0.4	–	–	–
Mar. 25, 2005	3	409	4	54	0	43

[a] Storm was in San Diego area only.

5. Discussion

This study shows that the data collected by "ocean color" satellites (e.g., MODIS-Aqua) are a useful tool for detection of stormwater plumes and the methods used in this study, including NIR-SWIR atmospheric correction and statistical methods of accuracy assessment, can be used in other coastal regions.

MODIS imagery can be used for estimation of the plume size and direction even in areas like the SCB, where plume size is much smaller than the plumes of large rivers like the Mississippi (Walker, 1996; DelCastillo et al., 2001; D'Sa and Miller, 2003), the Amazon (Curtin and Legeckis, 1986; Mertes et al., 1993; Del Vecchio and Subramaniam, 2004), the Orinoco (Muller-Karger et al., 1989), and the Columbia (Fiedler and Laurs, 1990). Ship-based data alone are inadequate to resolve the plume boundaries or to provide a synoptic view of the direction of propagation and offshore/alongshore extension of a plume. In all of the SCB regions, the areas covered by Bight'03 ship-based sampling were smaller than the areas of stormwater plumes detected by satellite sensors (cf. Warrick et al., 2007). This difference was largely by design given the expense and logistical difficulties of sampling such large regions. It was especially

Table 3
The size of the areas of impact (A; km^2) calculated on the basis of FIB exceedances by interpolating over the in situ sampling grid, and the size of total area sampled (T; km^2). Regions indicate outfalls of the rivers (see Table 2). The dates of surveys in Ventura, Santa Monica and San Pedro regions were different from San Diego region. The impact areas were significantly smaller than the plume areas shown in Table 2

Storm	Day after storm	FIB	Date of survey	Ventura (SCR + VR)		Santa Monica Bay (BC)		San Pedro (LAR + SGR + SAR + NB)		Date of survey	San Diego (SDR + TJR)	
				A	*T*	*A*	*T*	*A*	*T*		*A*	*T*
2004	1	Total coliforms	Feb. 27	0	93.8	–	–	7.8	131	Feb. 24	20.3	50
		Fecal coliforms		0	93.8	–	–	0	131		26.8	50
		Enterococcus		0	93.8	–	–	39.4	131		48.7	50
	2	Total coliforms	Feb. 28	–	–	0	48.2	22.3	272	Feb. 28	3	84
		Fecal coliforms		–	–	0	48.2	0	272		4.7	84
		Enterococcus		–	–	0	48.2	15.2	272		0	84
	3	Total coliforms	Feb. 29	–	–	–	–	–	–	Feb. 29	8.5	172
		Fecal coliforms		–	–	–	–	–	–		3.8	172
		Enterococcus		–	–	–	–	–	–		0	172
	4	Total coliforms	Mar. 1	–	–	0	48.2	0	272		–	–
		Fecal coliforms		–	–	0	48.2	0	272		–	–
		Enterococcus		–	–	0	48.2	5.7	272		–	–
2005	1	Total coliforms	Mar. 23	–		1.53	24.3	0	62	Feb. 13	51.9	53
		Fecal coliforms		–		0.05	24.3	0	62		51.9	53
		Enterococcus		–		0	24.3	5	62		51.9	53
	2	Total coliforms	Mar. 24	0	24.3	0.02	48.4	2.13	33	Feb. 14	50.3	53
		Fecal coliforms		0	24.3	0	48.4	0	33		42.9	53
		Enterococcus		0	24.3	0	48.4	0	33		51.9	53
	3	Total coliforms	Mar. 25	0	24.3	–	–	0	253	Feb. 15	103	126
		Fecal coliforms		0	24.3	–	–	0	146		63	126
		Enterococcus		0	24.3	–	–	4.4	253		70.5	126
	4	Total coliforms	Mar. 26	0	24.3	0	48.4	–	–		–	–
		Fecal coliforms		0	24.3	0	48	–	–		–	–
		Enterococcus		0	24.3	0	48	–	–		–	–

evident in the Ventura region, where plumes are typically larger than in the rest of the SCB (Nezlin et al., 2005), which can be explained by the large watershed area, high discharge volumes, the high concentration of discharged sediments (Otero and Siegel, 2004; Warrick et al., 2004c), and by the dynamic circulation patterns typical to that region (Harms and Winant, 1998; Bray et al., 1999).

The general plume characteristics revealed from SeaWiFS observations in 1997–2003 (Nezlin and DiGiacomo, 2005; Nezlin et al., 2005) are in accordance with the results of this study: the largest plumes were observed in the Ventura region and the smallest in Santa Monica Bay. Maximum plume size occurred 1 day after a rainstorm over the San Pedro Shelf and 2 days in other regions. The differences between SCB watersheds are illustrated by the comparison between ocean color imagery and the areas of FIB impact. In particular, a large natural watershed of the Ventura and Santa Clara Rivers more slowly released its water and FIB loads into the coastal waters, while a more urbanized large watershed off the Los Angeles (LA) and San Gabriel Rivers released the FIB load much faster due to channelized flow. Another factor regulating FIB impact in the San Pedro region is that the LA River and two major urban storm drain systems, Wilmington Drain and Dominguez Channel all enter into the greater Los Angeles/Long Beach Harbor, which is isolated from the coastal water by an extended breakwater. A smaller urban watershed off the Ballona Creek seemed to flash so fast and apparently with high enough dilution and dispersion of the plume that the elevated FIB area in the Santa Monica Bay was minimal. In all three of these cases the FIB supposedly originated from natural sources, i.e., non-human and not sewage. By contrast, the Tijuana River system looked very different and the FIB impact there was significantly higher than in other SCB coastal areas.

An important issue is the applicability of offshore water quality measurements, including satellite remote sensing, to water quality in the surf zone off the beach, where almost all human water contact happens. MODIS imagery analyzed in this study has a 1-km spatial resolution, and the optical signal of the ocean zone along the coastline (2–3 km) is affected by the "stray light effect", i.e., the sunlight reflected by land. As such, the satellite ocean color measurements cannot be directly attributed to beach water quality. However, satellite imagery provides important information about plume size and direction. In particular, it is evident from satellite imagery that channelized river systems that "shoot" runoff offshore where FIB rapidly decrease below recreational standards may be a highly efficient and cost-effective management for urban storm flow in southern California and other coastal regions.

Accurate discrimination between plumes and ocean waters was based on the entire visible spectrum, i.e., eight MODIS wavebands 412–748 nm. The optical signatures of plumes are modulated by two constituents contributing to ocean color: suspended sediments and CDOM. High concentrations of suspended sediments dominated by lithogenic silica (Toole and Siegel, 2001; Warrick et al., 2004b) increase backscattering in the central and to less extent longer wavelength portions of spectra (Otero and Siegel, 2004); CDOM absorbs light at short wavelengths (Del Castillo, 2005). As a result, the differences between nLw in plume and ocean are most evident for the 531–551 nm wavelengths, and are therefore the most informative for plume detection (at least in this region). Our previous studies of freshwater plumes in the SCB were based on SeaWiFS nLw of 555 nm wavelength (Nezlin and DiGiacomo, 2005; Nezlin et al., 2005).

Our results show that in remotely sensed plume detection, the chance to classify ocean as plume is higher than the chance to classify plume as ocean: for plume, commission errors exceeded omission errors. It was true for plumes determined both in terms of salinity and FIB exceedances. However, the accuracy of plume classification in terms of salinity is not directly transferable to FIB counts (i.e., water quality). In the SCB, the concentrations of total coliforms, fecal coliforms and *Enterococcus* in plume waters are typically higher in low salinity waters than in ambient ocean waters (Bay et al., 2003; Nezlin et al., 2007 Chapter 6), but the stations where FIB counts exceeded the California State Water Board standard often occurred beyond the plume limits. Low correlation between salinity and bacterial contamination is not surprising, because bacteria have a high mortality rate in sunlight (Davies and

Evison, 1991; Davies-Colley et al., 1994; Sinton et al., 2002; Noble et al., 2004) and may therefore decrease at a much faster rate than that due to mixing alone. Furthermore, bacteria concentrations are typically quite patchily distributed (e.g., Boehm and Weisberg, 2005; Rosenfeld et al., 2006). Meanwhile, an important assessment in terms of human health risk is the commission error for ocean water, i.e., the chance that areas classified as non-plume (~non-contaminated) waters, exceed the FIB contamination standard. This accuracy was as low as 13%, much lower than the commission error for plume (78%). This means that of the two types of errors (erroneous plume detection resulting in unjustified beach closures vs. undetected pathogen-laden plumes resulting in human health risk), the first error type looks more probable in remotely sensed plume monitoring and assessments.

Horizontal advection of plume waters as well as potential spatial inaccuracy of the MODIS-Aqua satellite imagery (pixel size 1 km) were not significant sources of plume detection errors. We hypothesized that if spatial inaccuracy was a significant factor, the accuracy of plume detection would increase after smoothing the satellite image increasing the areas from which classified pixels were selected. The accuracy statistics, however, were highest at a minimal (1.5 km) radius of circular areas around stations. This size was close to a 3×3 pixel box and smaller than the 5×5 pixel box recommended by Bailey and Werdell (2006) for spatially homogeneous ocean waters. Higher accuracy at smaller pixel box size may result from spatial heterogeneity typical of the coastal ocean. In this study, due to the limited number of stations, we compared all satellite and ship-based data collected on the same day and did not limit our analysis with a shorter time window, like the 6-h ($\pm$3-h) window recommended by Bailey and Werdell (2006). In other studies focused on the calibration and validation of remotely sensed data, the observations were considered a match (i.e., coming from a unique station) when all measurements were made within a 12-h window and within 0.05 degrees (5.6 km at the equator) in both latitude and longitude (Maritorena et al., 2006).

The combined NIR-SWIR atmospheric correction algorithm (Wang and Shi, 2007) was shown to be the best choice for detection of stormwater plumes in the SCB. Coastal waters (Case 2) are "optically complex" (Morel and Prieur, 1977) and atmospheric correction of satellite imagery requires more sophisticated approaches than open ocean waters (Siegel et al., 2000). The main difficulty is that the "black pixel assumption", i.e., the assumption that water-leaving radiance in near-infrared (NIR) is negligible, is true for clean oligotrophic ocean waters but typically does not work in coastal areas, where significant NIR backscattering results from high concentrations of phytoplankton and suspended sediments. In the open ocean, aerosol radiative properties can be determined from NIR remotely sensed reflectances, which contain a signal from the atmosphere (Gordon and Wang, 1994; Gordon, 1997). In turbid coastal waters, however, ocean color retrievals are imperfect, with significant errors in derived products often resulting from ocean contributions at the NIR bands (Wang, 2007; Wang et al., 2007). Using MODIS SWIR instead of NIR wavelengths for atmospheric correction is a promising method (Wang and Shi, 2005, 2006; Wang, 2007; Wang et al., 2007), because in the SWIR the ocean is generally black even in coastal regions due to much stronger water absorption (Hale and Querry, 1973). In non-turbid waters, however, the NIR method is preferable because the MODIS NIR bands have much better sensor SNR characteristics than the SWIR bands. The combined SWIR-NIR atmospheric correction method based on turbid water detection suggested by Shi and Wang (2007) was shown to be a good choice for processing of MODIS-Aqua imagery in coastal waters (Wang and Shi, 2007). This capability needs to be incorporated into ocean color processing on a routine, ideally operational, basis to support this and other important coastal management applications.

Overall system improvements in our ability to observe ocean color from satellites, especially increases in spatial, temporal and spectral resolutions, will greatly enhance our ability to use these observations as a tool for studying regional coastal processes and features such as stormwater runoff plumes, as well as harmful algal blooms (Schnetzer et al., 2007). Satellite data, even qualitative data (e.g., classified into "plume" and "ocean"), provide critical synoptic information (e.g., plume size and location) for coastal managers and decision-makers. This information cannot be obtained from ship-based sampling alone and its use needs to be promoted and facilitated wherever and whenever possible.

Along these lines, this study, and its companion papers detailing findings from the Bight '03 Regional Water Quality Program (Ahn et al., 2005; Nezlin et al., 2007; Warrick et al., 2007), provide an important step in incorporating ocean color satellite data into the water quality decision-support systems used by southern California coastal managers.

6. Conclusions

Satellite imagery is a useful tool for the estimation of the extent of polluted plumes, which is hardly achievable by direct sampling methods. A combined near-infrared/shortwave-infrared (NIR-SWIR) method of atmospheric correction of MODIS imagery substantially improves normalized water-leaving radiation (nLw) optical spectra in coastal waters with high turbidity. The total accuracy of plume detection in terms of surface salinity and/or FIB exceedances was not high (64–68%), seemingly because of imperfect correlations between ocean color, plume salinity and bacterial contamination. The chance to miss undetected pathogen-laden plumes resulting in human health risk was much lower than the chance of erroneous plume detection.

Acknowledgments

The authors would like to thank Wei Shi for help in processing MODIS data, and the NASA GSFC for the production and distribution of the MODIS data and images. MODIS data were acquired as part of the NASA's Earth Science Enterprise and were processed by the MODIS Adaptive Processing System (MODAPS), archived and distributed by the Goddard DAAC. The authors thank all participants of the Bight'03 Regional Water Quality Program. Critical comments of Alex Steele, Ivan Valiela and two anonymous reviewers helped to improve the paper significantly. We also thank Karlene Miller for editing the manuscript to make the writing style more accessible. This work was partly supported by a NASA Oceans & Ice Research Award (NRA-04-OES-02) from the NASA Ocean Biology and Biogeochemistry Program (Dr. Paula Bontempi, Program Scientist). The contents of this article are solely the opinions of the authors and do not constitute a statement of policy, decision, or position on behalf of the United States Geological Survey (USGS), the National Oceanic and Atmospheric Administration (NOAA) or the U.S. Government.

References

Ahn, J.H., Grant, S.B., Surbeck, C.Q., DiGiacomo, P.M., Nezlin, N.P., Jiang, S., 2005. Coastal water quality impact of stormwater runoff from an urban watershed in southern California. Environmental Science & Technology 39, 5940–5953.

Bailey, S.W., Werdell, P.J., 2006. A multi-sensor approach for the on-orbit validation of ocean color satellite data products. Remote Sensing of Environment 102, 12–23.

Bay, S., Jones, B.H., Schiff, K., Washburn, L., 2003. Water quality impacts of stormwater discharges to Santa Monica Bay. Marine Environmental Research 56, 205–223.

Boehm, A.B., Weisberg, S.B., 2005. Tidal forcing of enterococci at marine recreational beaches at fortnightly and semidiurnal frequencies. Environmental Science & Technology 39, 5575–5583.
Bray, N.A., Keyes, A., Morawitz, W.M.L., 1999. The California current system in the Southern California Bight and the Santa Barbara Channel. Journal of Geophysical Research-Oceans 104, 7695–7714.
Congalton, R.G., Green, K., 1999. Assessing the Accuracy of Remotely Sensed Data: Principles and Practices. Lewis Publishers, Boca Raton, 137 pp.
Curtin, T.B., Legeckis, R.V., 1986. Physical observations in the plume region of the Amazon River during peak discharge. I. Surface variability. Continental Shelf Research 6, 31–51.
D'Sa, E.J., Miller, R.L., 2003. Bio-optical properties in waters influenced by the Mississippi River during low flow conditions. Remote Sensing of Environment 84, 538–549.
Dailey, M.D., Anderson, J.W., Reish, D.J., Gorsline, D.S., 1993. The Southern California Bight: background and setting. In: Dailey, M.D., Reish, D.J., Anderson, J.W. (Eds.), Ecology of the Southern California Bight. University of California Press, Berkeley, pp. 1–18.
Davies-Colley, R.J., Bell, R.G., Donnison, A.M., 1994. Sunlight inactivation of enterococci and fecal coliforms in sewage effluent diluted in seawater. Applied and Environmental Microbiology 60, 2049–2058.
Davies, C.M., Evison, L.M., 1991. Sunlight and the survival of enteric bacteria in natural waters. Journal of Applied Microbiology 70, 265–274.
Del Castillo, C.E., 2005. Remote sensing of organic matter in coastal waters. In: Miller, R.L., Del Castillo, C.E., McKee, B.A. (Eds.), Remote Sensing of Coastal Aquatic Environments. Technologies, Techniques and Applications. Springer, Dordrecht, pp. 157–180.
Del Vecchio, R., Subramaniam, A., 2004. Influence of the Amazon River on the surface optical properties of the western tropical North Atlantic Ocean. Journal of Geophysical Research-Oceans 109, C11001.
DelCastillo, C.E., Coble, P.G., Conmy, R.N., Muller-Karger, F.E., Vanderbloemen, L., Vargo, G.A., 2001. Multispectral in situ measurements of organic matter and chlorophyll fluorescence in seawater: documenting the intrusion of the Mississippi River plume in the West Florida Shelf. Limnology and Oceanography 46, 1836–1843.
Esaias, W.E., Abbott, M.R., Barton, I., Brown, O.B., Campbell, J.W., Carder, K.L., Clark, D.K., Evans, R.H., Hoge, F.E., Gordon, H.R., Balch, W.M., Letteller, R.M., Minnett, P.J., 1998. An overview of MODIS capabilities for ocean science observations. IEEE Transactions on Geoscience and Remote Sensing 36, 1250–1265.
Estournel, C., Kondrachoff, V., Marsaleix, P., Vehil, R., 1997. The plume of the Rhone: numerical simulation and remote sensing. Continental Shelf Research 17, 899–924.
Fiedler, P.C., Laurs, R.M., 1990. Variability of the Columbia River plume observed in visible and infrared satellite imagery. International Journal of Remote Sensing 11, 999–1010.
Froidefond, J.-M., Jegou, A.-M., Hermida, J., Lazure, P., Castaing, P., 1998. Variability of the Gironde turbid plume by remote sensing. Effects of climatic factors. Oceanologica Acta 21, 191–207.
Gordon, H.R., 1997. Atmospheric correction of ocean color imagery in the Earth Observing System era. Journal of Geophysical Research-Atmospheres 102, 17081–17106.
Gordon, H.R., Wang, M., 1994. Retrieval of water-leaving radiance and aerosol optical thickness over the oceans with SeaWiFS: a preliminary algorithm. Applied Optics 33, 443–452.
Hale, G.M., Querry, M.R., 1973. Optical constants of water in the 200-nm to 200-micrometer wavelength region. Applied Optics 12, 555–563.
Harms, S., Winant, C.D., 1998. Characteristic patterns of the circulation in the Santa Barbara Channel. Journal of Geophysical Research-Oceans 103, 3041–3065.
Hickey, B.M., 1993. Physical oceanography. In: Dailey, M.D., Reish, D.J., Anderson, J.W. (Eds.), Ecology of the Southern California Bight. University of California Press, Berkeley, pp. 19–70.
Lillesand, T.M., Kiefer, R.W., 2000. Remote Sensing and Image Interpretation, fourth ed. John Wiley & Sons, New York, 724 pp.
Lira, J., Morales, A., Zamora, F., 1997. Study of sediment distribution in the area of the Panuco river plume by means of remote sensing. International Journal of Remote Sensing 18, 171–182.
Lynn, R.J., Bograd, S.J., Chereskin, T.K., Huyer, A., 2003. Seasonal renewal of the California Current: the spring transition off California. Journal of Geophysical Research-Oceans 108, 3279.
Maritorena, S., Lee, Z., Du, K., Loisel, H., Doerffer, R., Roesler, C.S., Lyon, P.E., Tanaka, A., Babin, M., Kopelevich, O.V., 2006. Synthetic and in situ data sets for algorithm testing. In: Lee, Z. (Ed.), Remote Sensing of Inherent Optical Properties: Fundamentals, Tests of Algorithms and Applications, vol. 5. IOCCG, Dartmouth, Canada, pp. 13–18.
Mertes, L.A.K., Warrick, J.A., 2001. Measuring flood output from 110 coastal watersheds in California with field measurements and SeaWiFS. Geology 29, 659–662.
Mertes, L.A.K., Smith, M.O., Adams, J.B., 1993. Estimating suspended sediment concentrations in surface waters of the Amazon River wetlands from Landsat images. Remote Sensing of Environment 43, 281–301.
Miller, R.L., McKee, B.A., 2004. Using MODIS Terra 250 m imagery to map concentrations of total suspended matter in coastal waters. Remote Sensing of Environment 93, 259–266.
Miller, R.L., McKee, B.A., D'Sa, E.J., 2005. Monitoring bottom sediment resuspension and suspended sediments in shallow coastal waters. In: Miller, R.L., Del Castillo, C.E., McKee, B.A. (Eds.), Remote Sensing of Coastal Aquatic Environments. Springer, Dordrecht, pp. 259–276.
Miller, S.N., Kepner, W.G., Mehaffey, M.H., Hernandez, M., Miller, R.C., Goodrich, D.C., Devonald, K.K., Heggem, D.T., Miller, W.P., 2002. Integrating landscape assessment and hydrologic modeling for land cover change analysis. Journal of the American Water Resources Association 38, 915–929.
Monahan, E.C., Pybus, M.J., 1978. Colour, UV absorbance and salinity of the surface waters off the west coast of Ireland. Nature 274, 782–784.
Morel, A., Prieur, L., 1977. Analysis of variations in ocean color. Limnology and Oceanography 22, 709–722.
Muller-Karger, F.E., McClain, C.R., Fisher, T.R., Esaias, W.E., Varela, R., 1989. Pigment distribution in the Caribbean Sea: observations from space. Progress in Oceanography 23, 23–64.
Nezlin, N.P., DiGiacomo, P.M., 2005. Satellite ocean color observations of stormwater runoff plumes along the San Pedro Shelf (southern California) during 1997–2003. Continental Shelf Research 25, 1692–1711.
Nezlin, N.P., DiGiacomo, P.M., Stein, E.D., Ackerman, D., 2005. Stormwater runoff plumes observed by SeaWiFS radiometer in the Southern California Bight. Remote Sensing of Environment 98, 494–510.
Nezlin, N.P., DiGiacomo, P.M., Weisberg, S.B., Diehl, D.W., Warrick, J.A., Mengel, M.J., Jones, B.H., Reifel, K.M., Johnson, S.C., Ohlmann, J.C., Washburn, L., Terrill, E.J., 2007. Southern California Bight 2003 Monitoring Program: V. Water Quality. Southern California Coastal Water Research Project, Costa Mesa, 157 pp.
Noble, R.T., Lee, I.M., Schiff, K.C., 2004. Inactivation of indicator bacteria from various sources of fecal contamination in seawater and freshwater. Journal of Applied Microbiology 96, 464–472.
Noble, R.T., Weisberg, S.B., Leecaster, M.K., McGee, C.D., Dorsey, J.H., Vainik, P., Orozco-Borbon, V., 2003. Storm effects on regional beach water quality along the southern California shoreline. Journal of Water and Health 1, 23–31.
Opsahl, S., Benner, R., 1998. Photochemical reactivity of dissolved lignin in river and ocean waters. Limnology and Oceanography 43, 1297–1304.
Otero, M.P., Siegel, D.A., 2004. Spatial and temporal characteristics of sediment plumes and phytoplankton blooms in the Santa Barbara Channel. Deep-Sea Research II 51, 1129–1149.
Ouillon, S., Forget, P., Froidefond, J.-M., Naudin, J.-J., 1997. Estimating suspended matter concentrations from SPOT data and from field measurements in the Rhone river plume. Marine Technology Society Journal 31, 15–20.
Richards, J.A., 1999. Remote Sensing Digital Image Analysis. Springer-Verlag, Berlin, 240 pp.
Rosenfeld, L.K., McGee, C.D., Robertson, G.L., Noble, M.A., Jones, B.H., 2006. Temporal and spatial variability of fecal indicator bacteria in the surf zone off Huntington Beach, CA. Marine Environmental Research 61, 471–493.
Schiff, K.C., Allen, M.J., Zeng, E.Y., Bay, S.M., 2000. Southern California. Marine Pollution Bulletin 41, 76–93.
Schnetzer, A., Miller, P.E., Schaffner, R.A., Stauffer, B.A., Jones, B.H., Weisberg, S.B., DiGiacomo, P.M., Berelson, W.M., Caron, D.A., 2007. Blooms of *Pseudo-nitzschia* and domoic acid in the San Pedro Channel and Los Angeles harbor areas of the Southern California Bight, 2003–2004. Harmful Algae 6, 372–387.
Shi, W., Wang, M., 2007. Detection of turbid waters and absorbing aerosols for the MODIS ocean color data processing. Remote Sensing of Environment 110, 149–161.
Siddorn, J.R., Bowers, D.G., Hoguane, A.M., 2001. Detecting the Zambezi River plume using observed optical properties. Marine Pollution Bulletin 42, 942–950.
Siegel, D.A., Wang, M., Maritorena, S., Robinson, W., 2000. Atmospheric correction of satellite ocean color imagery: the black pixel assumption. Applied Optics 39, 3582–3591.
Siegel, H., Gerth, M., Mutzke, A., 1999. Dynamics of the Oder river plume in the Southern Baltic Sea: satellite data and numerical modelling. Continental Shelf Research 19, 1143–1159.
Sinton, L.W., Hall, C.H., Lynch, P.A., Davies-Colley, R.J., 2002. Sunlight inactivation of fecal indicator bacteria and bacteriophages from waste stabilization pond effluent in fresh and saline waters. Applied and Environmental Microbiology 68, 1122–1131.
State Water Resources Control Board, 2005. California Ocean Plan, 57 pp.
Strub, P.T., James, C., 1988. Atmospheric conditions during the spring and fall transition in the coastal ocean off western United States. Journal of Geophysical Research-Oceans 93, 15561–15584.
Strub, P.T., Allen, J.S., Huyer, A., Smith, R.L., 1987. Large-scale structure of the spring transition in the coastal ocean off western North America. Journal of Geophysical Research-Oceans 92, 1527–1544.
Toole, D.A., Siegel, D.A., 2001. Modes and mechanisms of ocean color variability in the Santa Barbara Channel. Journal of Geophysical Research-Oceans 106, 26985–27000.
Vasilkov, A.P., Burenkov, V.I., Ruddick, K.G., 1999. The spectral reflectance and transparency of river plume waters. International Journal of Remote Sensing 20, 2497–2508.
Vodacek, A., Blough, N.V., DeGrandpe, M.D., Peltzer, E.T., Nelson, R.K., 1997. Seasonal variation of CDOM and DOC in the Middle Atlantic Bight: terrestrial inputs and photooxidation. Limnology and Oceanography 42, 674–686.
Walker, N.D., 1996. Satellite assessment of Mississippi River plume variability: causes and predictability. Remote Sensing of Environment 58, 21–35.
Wang, M., 2007. Remote sensing of the ocean contributions from ultraviolet to near-infrared using the shortwave infrared bands: simulations. Applied Optics 46, 1535–1547.
Wang, M., Shi, W., 2005. Estimation of ocean contribution at the MODIS near-infrared wavelengths along the east coast of the U.S.: two case studies. Geophysical Research Letters 32, L13606.

Wang, M., Shi, W., 2006. Cloud masking for ocean color data processing in the coastal regions. IEEE Transactions on Geoscience and Remote Sensing 44, 3196–3205.
Wang, M., Shi, W., 2007. The NIR-SWIR combined atmospheric correction approach for MODIS ocean color data processing. Optics Express 15, 15722–15733.
Wang, M., Tang, J., Shi, W., 2007. MODIS-derived ocean color products along the China east coastal region. Geophysical Research Letters 34, L06611.
Warrick, J.A., Milliman, J.D., 2003. Hyperpycnal sediment discharge from semiarid southern California rivers: implications for coastal sediment budgets. Geology 31, 781–784.
Warrick, J.A., Fong, D.A., 2004. Dispersal scaling from the world's rivers. Geophysical Research Letters 31. L04301.
Warrick, J.A., Mertes, L.A.K., Washburn, L., Siegel, D.A., 2004a. Dispersal forcing of southern California river plumes, based on field and remote sensing observations. Geo-Marine Letters 24, 46–52.
Warrick, J.A., Mertes, L.A.K., Washburn, L., Siegel, D.A., 2004b. A conceptual model for river water and sediment dispersal in the Santa Barbara Channel, California. Continental Shelf Research 24, 2029–2043.
Warrick, J.A., Mertes, L.A.K., Siegel, D.A., MacKenzie, C., 2004c. Estimating suspended sediment concentrations in turbid coastal waters of the Santa Barbara Channel with SeaWiFS. International Journal of Remote Sensing 25, 1995–2002.
Warrick, J.A., DiGiacomo, P.M., Weisberg, S.B., Nezlin, N.P., Mengel, M.J., Jones, B.H., Ohlmann, J.C., Washburn, L., Terrill, E.J., Farnsworth, K.L., 2007. River plume patterns and dynamics within the Southern California Bight. Continental Shelf Research 27, 2427–2448.
Washburn, L., Jones, B.H., Bratkovich, A.W., Dickey, T.D., Chen, M.-S., 1992. Mixing, dispersion, and resuspension in vicinity of ocean wastewater plume. Journal of Hydraulic Engineering-ASCE 118, 38–58.